Topological Analysis of the Experimental Electron Densities of Amino Acids. 1. D,L-Aspartic Acid at 20 K

R. Flaig, T. Koritsanszky, D. Zobel, and P. Luger*

Contribution from the Institute for Crystallography, Free University of Berlin, Takustrasse 6, 14195 Berlin, Germany

Received July 31, 1997. Revised Manuscript Received November 11, 1997

Abstract: High-resolution X-ray diffraction data collected at 20 K are interpreted in terms of the rigid-pseudoatom formalism to derive the electron density and related properties, such as the electrostatic potential and electric moments, of the crystalline D,L-aspartic acid. The refinement models applied are restricted via rigid-bond type constraints to reduce possible bias in the mean-square displacement amplitudes due to inadequacies in the thermal deconvolution. The density and its Laplacian extracted from the data is analyzed in terms of the topological properties of covalent bonds and nonbonded interactions. The results are compared to those calculated at the Hartree−Fock level of theory and to those obtained experimentally for analogous molecules. The comparison must consider the differences in the locations of the bond critical points of the densities in question, that is, how the bond polarity manifests itself in the distribution of charge obtained by different methods. One of the key questions to the reliability of experimental pseudoatomic densities seems to be whether the treatment of the X-ray data can be standardized so as to reduce model inadequacies, especially those related to the derivation of monopole populations.

Introduction

Based on Bader's approach,[1] all structural and chemical properties of molecules can be deduced from the topology of their distribution of electronic charge. An important aspect of the theory of atoms in molecules is that it provides atomic partitioning based on the electron density $\rho(\boldsymbol{r})$, a physical observable. An atom can be defined in terms of its boundary given by the gradient vector field of the molecular charge distribution. Physical properties of an atom defined in such a way are obtained as quantum mechanical averages of the corresponding observable over the atomic basin. The generalization of this atomic concept leads to the quantum definition of molecular residues recognized as functional groups in chemistry. It is the subject of ongoing research to build macromolecules from such density based monomers extracted from analogous smaller molecules through the topological analysis of their distribution of charge.[2,3] The key question to the theoretical construction of polymers is the transferability of the monomers, i.e., to what extent the interatomic surfaces, at which the fragments are linked to each other, remain undeformed in a slightly different chemical environment.[3] In this respect, the invariance of the characteristics of the bonds formed between the residues is essential. Atomic interactions in a molecule can be characterized by the local topological parameters of $\rho(\boldsymbol{r})$.[4,5] These are the value of $\rho(\boldsymbol{r}_b)$ and its Laplacian $\nabla^2\rho(\boldsymbol{r}_b)$, at the bond critical point (CP, located at $\boldsymbol{r}_b$ where $\nabla\rho(\boldsymbol{r}_b) = 0$), the bond path length l_b (the length of the maximum density path between the nuclei), and the ellipticity ϵ (a measure for the deviation of the charge density at the bond critical point from axial symmetry).

There is, on the one hand, growing evidence that the static $\rho(\boldsymbol{r})$ extracted from X-ray diffraction data can be reliable enough to provide topological characterization of different covalent bonds and nonbonded interactions.[6−10] On the other hand, the extent to which these topological properties are reproducible depends not only on experimental conditions but also on the interpretation of the data.[11−13] On the one hand, there seems to be an urgent need for experimental verification of the theoretical results, on the other hand, the proper treatment of the diffraction data needs increasing support from theory. The procedure of experimental charge density determination involves modeling of Bragg intensities in terms of the thermal average of $\rho(\boldsymbol{r})$.[14] The formalism relies on a series of approximations not directly deducable from the experiment. The goal is to extract an analytical static $\rho(\boldsymbol{r})$ expressed in terms of pseudoatomic densities which are expanded over nuclear-centered spherical harmonics (or related functions) augmented with properly chosen radial functions.[15,16] The density param-

(1) Bader, R. F. W. Atoms in Molecules − A Quantum Theory. Clarendon Press: Oxford, 1990.
(2) Chang, C.; Bader, R. F. W. *J. Phys. Chem.* **1992**, *96*, 1654.
(3) Popelier, P. L. A.; Bader, R. F. W. *J. Phys. Chem.* **1994**, *98*, 4473.
(4) Bader, R. F. W.; Slee, T. S.; Cremer, D.; Kraka, E. *J. Am. Chem. Soc.* **1983**, *105*, 5061.
(5) Cremer, D.; Kraka, E.; Slee, T. S.; Bader, R. F. W.; Lau, C. D. H.; Nguyen-Dang, T. T.; MacDougall, P. J. *J. Am. Chem. Soc.* **1983**, *105*, 5069.
(6) Lau, C. O. H.; Bader, R. F. W.; Hermansson, K.; Berkovitch-Yellin *Chem. Scr. Abstr.* **1986**, *26*, 476.
(7) Kappkhan, M. Tsirel'son, V. G.; Ozerov, R. P. *Dokl. Phys. Chem.* **1989**, *303*, 1025.
(8) Gatti, C.; Bianchi, R.; Destro, R.; Merati, F. *J. Mol. Struct. (THEOCHEM)* **1992**, *255*, 409.
(9) Flensburg, C.; Larsen, S.; Stewart, R. F. *J. Phys. Chem.* **1995**, *99*, 10130.
(10) Koritsanszky, T.; Buschmann, J.; Luger, P. *J. Phys. Chem.* **1996**, *100*, 10547.
(11) Fuhrmann, P.; Koritsanszky, T.; Luger, P. *Zeitschrift Kristallogr.* **1997**, *212*, 213.
(12) Koritsanszky, T.; Zobel, D.; Luger, P. J. Phys. Chem. **1997**, submitted.
(13) Howard, S. T.; Hursthouse, M. B.; Lehmann, C. W.; Poyner, E. A. *Acta Crystallogr.* **1995**, *B51*, 328.
(14) Stewart, R. F.; Feil, D. *Acta Crystallogr.* **1980**, *A36*, 503.
(15) Stewart, R. F. *J. Chem. Phys.* **1973**, *58*, 1668.

S0002-7863(97)02620-6 CCC: $15.00
Published on Web 03/03/1998

eters are obtained by least-squares (LSQ) fitting of the model predicted structure factor amplitudes to those measured. Hidden indeterminacies in the variables, model inadequacies, and low resolution of the data bias the parameter estimates. The applicability of the usual statistical figures of the fit in judging the correctness of the model is very limited, and many studies are concerned about testing the physical significance of the outcomes.

Our aim with a series of charge density studies on amino acids is in accord with these introductory remarks. The primary interest is to find the optimal parametrization and the refinement strategy best suited for this type of compounds. A special attention will be paid to the proper thermal deconvolution, the treatment of the hydrogen atoms and chemical constraints. A standardized interpretation of data collected under similar experimental conditions on chemical analogues is believed to access the reliability and reproducibility of the technique. The final goal is to derive methodologically self-consistent experimental electronic properties of these molecules as well as of their analogous functional groups based on the topology of $\rho(\boldsymbol{r})$. In the first stage the Laplacian function, the electrostatic potential (EP), and dipole and quadrupole moments will be evaluated and compared to the outcomes of quantum chemical calculations. Such efforts should be extended to larger molecules of biological importance.

A survey based on the Cambridge Database shows that the 20 naturally occurring α-amino acids in their zwitterionic form have been extensively studied by diffraction techniques. Neutron structural data are available for 16 compounds out of 20, most of them are based on room temperature measurements, except for asparagine (15 K) and glycine (83 K). Despite the importance of this class of compounds only very few studies have been performed on the determination of their experimental charge distribution. The 120 K X-ray data of glycine have been interpreted in terms of conventional deformation densities[17] and, more recently, by using the two-channel maximum entropy method.[18] Preliminary results of the charge density of D,L-histidine obtained from serial and imaging plate data registration have also been reported.[19] Detailed and well documented studies, including the topological analysis of $\rho(\boldsymbol{r})$ exist on L-alanine based on data collected at 23 K.[8]

The crystal and molecular structure of D,L-aspartic acid was determined by Rao et al., first from photographic intensities[20] and then by using single-crystal diffraction technique.[21] The latest structural work is a neutron study at room temperature.[22] The results reported here are based on the data which are, to our best knowledge, the most extensive ones ($\sin(\theta)/\lambda = 1.3678$ Å^{-1}) collected at 20 K with a conventional X-ray source (AgK_α) and a solid state detector. X-ray data of the same quality have recently been collected and are being analyzed for L-threonine. A preliminary report on the experimental charge density of L- and D,L-serine can be found in ref 23.

Table 1. Summary of Crystallographic Data and Experimental Conditions

formula	$C_4H_7NO_4$
crystal system	monoclinic
space group	*C*2/*c*
Z	8
temp (K)	20(1)
a (Å)	18.904(4)
b (Å)	7.337(5)
c (Å)	9.138(2)
β (deg)	123.45(1)
V (Å^3)	1057.49
F(000)	560
D_x (g/cm^3)	1.62
crystal size (mm^3)	0.31 × 0.40 × 0.52
radiation	AgK_α, Pd filter
λ (Å)	0.5609
μ (cm^{-1})	0.958
abs. factor min/max	1.020/1.043
scan type	$\omega-2\theta$
step width $\Delta 2\theta\Delta\omega$ (deg)	0.04/0.02
scan width $\Delta\omega$ (deg)	0.94−1.43
time per step min/max (s)	0.3/3.0
standard reflections	$(\bar{2}\bar{2}3)$, $(\bar{3}\bar{5}\bar{1})$, $(7\bar{3}\bar{3})$
interval for standards (min)	90
$(\sin\theta/\lambda)_{max}$ (Å^{-1})	1.3678
N_{measured}	13340
N_{unique}	11008 (2σ)
N_{unique}	7962 (3σ)
R_{merging}	0.0106

Experimental Section

The crystal used for the measurement was obtained by crystallization of the commercially available product from an aqueous solution. The measurement was performed on a large four-circle Eulerian cradle (Huber, type 512) equipped with a double-stage closed-cycle He refrigerator (Displex, Air Products, USA) and a Be vacuum chamber around the cold head. The crystal was mounted on a special Be-needle carrier[24] and cooled to 20 K with a cooling rate of 1 K min^{-1}. During the cooling procedure several reflections were monitored by ω-scans to control the crystal quality. The alignment of the crystal was controlled by the C8 routine, based on centering of one reflection in eight equivalent positions.[25] AgK_α radiation was used at 55 kV and 36 mA, which made it possible to have a resolution of up to 1.368 Å^{-1} in $\sin\theta/\lambda$. For the intensity measurement a solid-state detector, containing a Li-drifted Si-target (12 mm ø) cooled together with the preamplifier with liquid N_2, was used. This type of detector shows a large quantum efficiency with an energy resolution up to 140 eV. We selected one with about 600 eV at 22 keV (fwhm) because the difference of 160 eV between $K_{\alpha1} - K_{\alpha2}$ for Ag-radiation is too small to separate and therefore should be registered together. The electronic window of a single channel analyzer was tuned carefully to the position of the $K_{\alpha1/\alpha2}$-doublet, so that the K_β-line could be suppressed. The use of this solid state detector resulted in better counting statistics and signal-to-noise ratio, especially for the high order reflections, compared to a conventional scintillation counter. The cell dimensions and the orientation matrix used during the data collection were obtained by least-squares refinement on 39 centered reflections with $49° < 2\theta < 60°$. Three standard reflections were selected to monitor the intensities in 90 min intervals during the measurement. The data were scaled according to the change in intensities of the standard reflections and corrected for Lorentz and polarization effects. An analytical absorption correction was also applied.[26] The internal merging index for averaging the symmetry equivalent reflections was $R_{int} = 0.0106$. Further details on crystal data and experimental conditions can be found in Table 1.

(16) Hansen, N. K.; Coppens, P. *Acta Crystallogr.* **1978**, *A34*, 909.
(17) Legros, J.-P.; Kvick, A. *Acta Crystallogr.* **1980**, *B36*, 3052.
(18) Papoular, R. J.; Vekhter, Y.; Coppens, P. *Acta Crystallogr.* **1996**, *A52*, 397.
(19) Carducci, M.; Bolotovsky, R.; Coppens, P. *Acta Crystallogr.* **1996**, *A52*.
(20) Rao, S.-T.; Srinivasan R.; Valambal V. *Pure Appl. Phys. (India)* **1968**, *6*, 523.
(21) Rao, S.-T. *Acta Crystallogr.* **1973**, *B29*, 1718.
(22) Sequeira, A.; Rajagopal, H.; Ramanadham, M. *Acta Crystallogr.* **1989**, *C45*, 906.
(23) Buschmann, J.; Koritsanszky, T.; Ramm, M.; Luger, P. *Acta Crystallogr.* **1996**, A52.
(24) Zobel, D.; Luger, P. J. *Appl. Crystallogr.* **1990**, *23*, 175.
(25) King, H. E.; Finger, L. W. J. *Appl. Crystallogr.* **1979**, *12*, 374.
(26) Coppens, P.; Hamilton, W. C. *Acta Crystallogr.* **1970**, *A26*, 71.

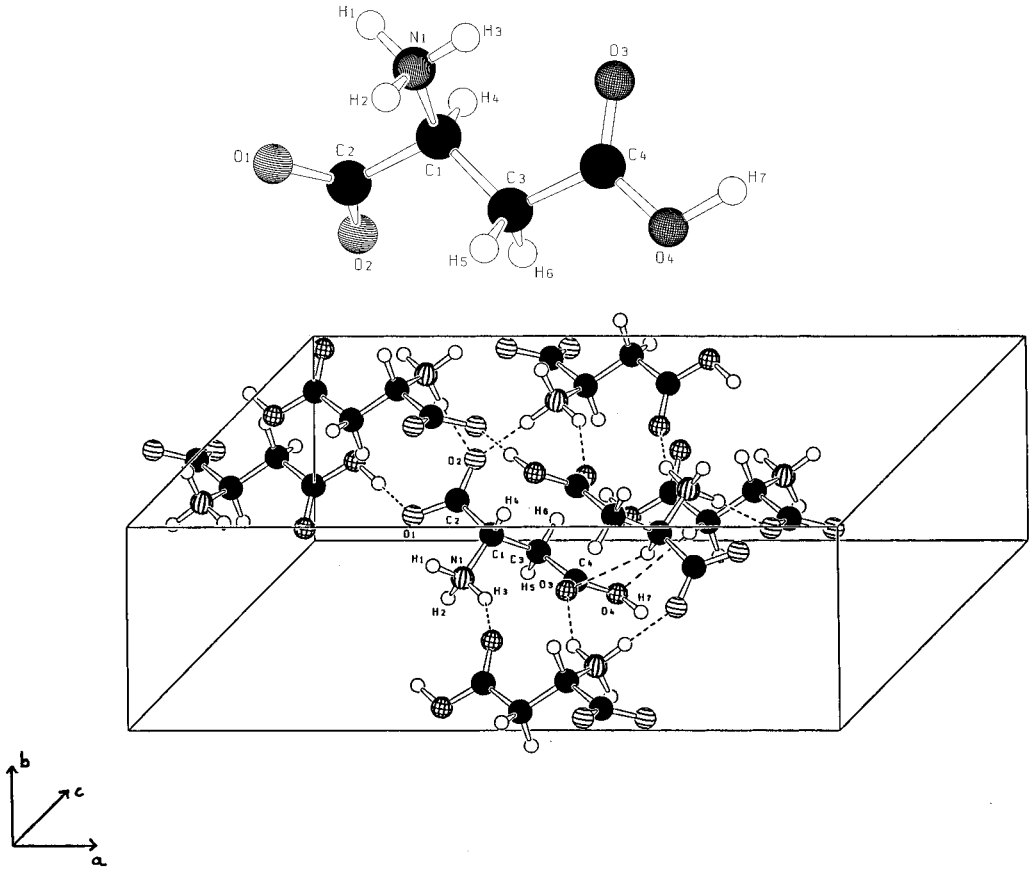

Figure 1. D,L-Aspartic acid in the crystal, SCHAKAL representations:[46] (a) molecular structure with atom numbering and (b) part of the crystal lattice illustrating the intermolecular interactions (dashed lines), see also Table 10.

Theoretical Calculations

Ab initio calculations were performed with the GAUSSIAN92 program package[27] at the Hartree−Fock (HF) level of theory. Full optimizations were carried out with the 6-311G** basis set starting from the X-ray structural data. As convergence criterion the threshold limits of 0.000 45 and 0.001 8 au were applied for the maximum force and displacement, respectively. The optimizations were followed by the evaluation of the harmonic vibrational frequencies (HF) and internal vibrational amplitudes.[28] The topological analyses were based on the wave functions obtained from single point calculations using different standard basis sets. These calculations were based on the experimental geometry with optimized C−H, O−H, and N−H distances.

Density Models and Refinement Strategy

The generalized scattering factor model based on the Hansen-Coppens formalism was applied.[16] The starting atomic parameters were taken from a room-temperature neutron diffraction study.[22] The refinements were carried out with the full-matrix LSQ program (XDLSM) of the XD program package.[29]

In all cases the quantity $\sum_{\mathbf{H}} w_{\mathbf{H}}(|F_{\mathrm{obs}}(\mathbf{H})| - K|F_{\mathrm{cal}}(\mathbf{H})|)^2$ was minimized using the statistical weight $w_{\mathbf{H}} = \sigma^{-2}(F_{obs}(\mathbf{H}))$ and only those structure factors which met the criterion of $F_{obs}(\mathbf{H}) > 3\sigma(F_{obs}(\mathbf{H}))$. Common to all refinement models applied are the following conditions. The core and the spherical valence density was composed of Hartree−Fock wave functions expanded over Slater type basis functions.[30] For each heavy atom a different radial screening parameter (κ) was assigned and refined. The scattering factors of the hydrogen atoms were calculated from the exact radial density functions using $\kappa = 1.2$. This contraction allows a simple analytical approximation to the scattering factors introduced by Stewart et al.[31] For the deformation terms single-ζ orbitals with energy-optimized Slater exponents were taken and kept fixed.[30] The level of the expansion was hexadecapolar and dipolar for the heavy and for the hydrogen atoms, respectively. A bond directed quadrupole ($l = 2$, $m = 0$) was also introduced for the hydrogen atom of the O−H group. The atomic numbering used is shown in Figure 1, while the definition of the atomic site coordinate systems can be found in Table 2. A local mirror symmetry was implemented for the carbon atoms in the carboxyl, carboxylate, and methylene groups. The densities of the hydrogen atoms of the latter group were constrained to be the same. The molecule was kept neutral during the refinement (neutrality constraint). Several different isotropic extinction refinements[32] were perfomed, but the results showed no indication for the need of such correction. The results based on three models

(27) Frisch, M. J.; Trucks, G. W.; Schlegel, H. B.; Gill, P. M. W.; Johnson, B. G.; Wong, M. W.; Foresman, J. B.; Robb, M. A.; Head-Gordon, M.; Replogle, E. S.; Gomperts, R.; Andres, J. L.; Raghavachari, K.; Binkley, J. S.; Gonzalez, C.; Martin, R. L.; Fox, D. J.; Defrees, D. J.; Baker, J.; Stewart, J. J. P.; Pople, J. A. Gaussian 92/DFT, Revision G.1; Gaussian Inc.: Pittsburgh, PA, 1993.

(28) Higgs, P. W. Acta Crystallogr. **1955**, *8*, 99.

(29) Koritsanszky, T.; Howard, S.; Richter, T.; Su, Z.; Mallinson, P. R.; Hansen, N. K. XD − a Computer Program Package for Multipole Refinement and Analysis of Electron Densities from Diffraction Data. User Manual. Free University: Berlin, 1995.

(30) Clementi, E.; Roetti, C. Atomic Data and Nuclear Data Tables **1974**, *14*, 177.

(31) Stewart, R. F.; Davidson, E. R.; Simpson, W. T. *J. Chem. Phys.* **1965**, *42*, 3175.

(32) Becker, P. J.; Coppens. P. *Acta Crystallogr*. **1974**, *30*, 129.

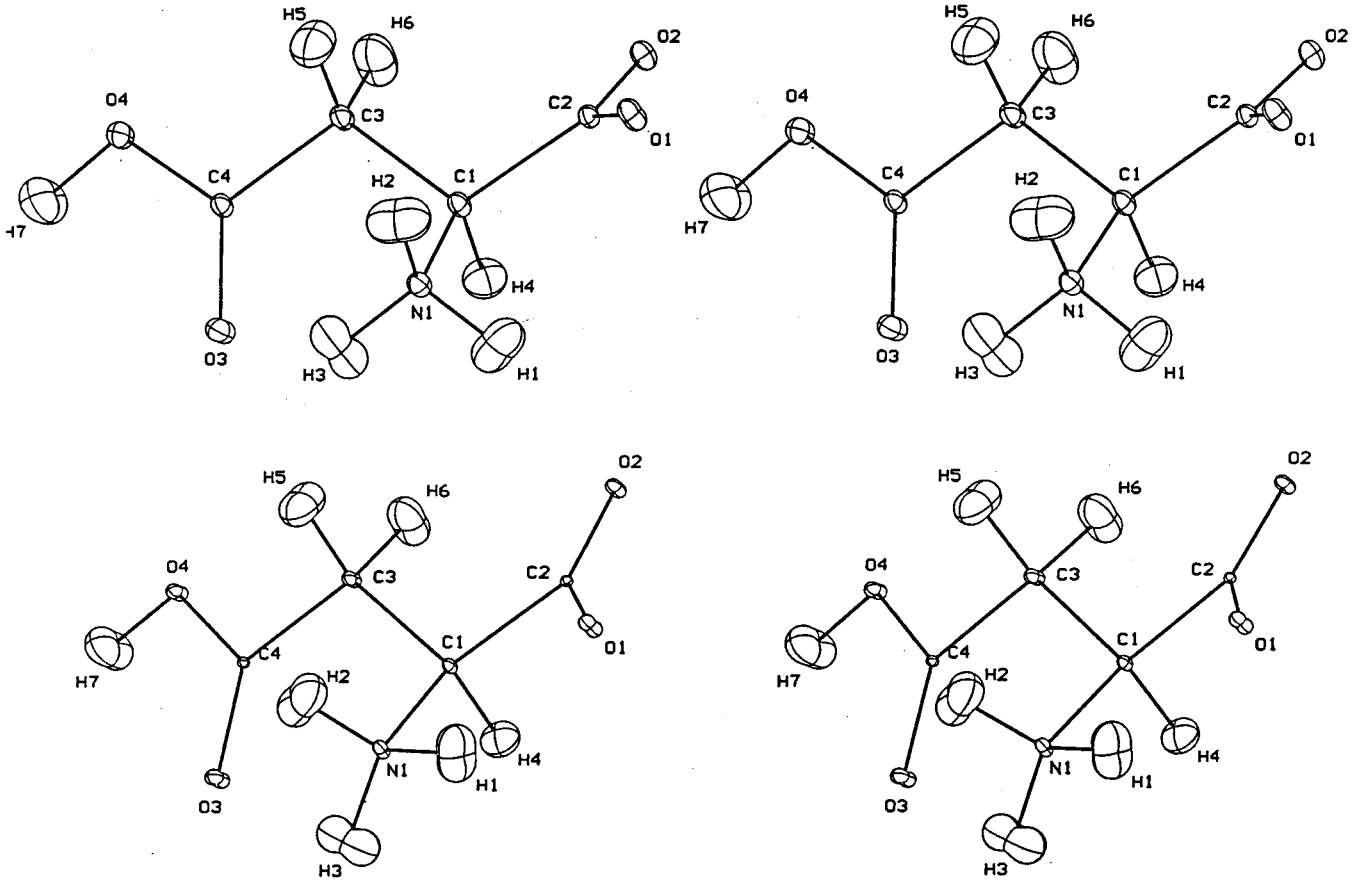

Figure 2. Stereo representation (PEANUT)[35] of the residual ADPs for the experimental (a) and optimized (b) molecular structure in terms of their root-mean-square displacement surfaces.

Table 2. Definition of the Local Atomic Coordinate System[a]

ATOM	ATOM 0	AX 1	ATOM 1	ATOM 2	AX 2
O(1)	C(2)	X	O(1)	O(2)	Y
O(2)	C(2)	X	O(2)	O(1)	Y
O(3)	C(4)	X	O(3)	O(4)	Y
O(4)	C(4)	X	O(4)	H(7)	Y
N(1)	C(1)	Z	N(1)	H(1)	X
C(1)	C(2)	Z	C(1)	O(1)	Y
C(2)	C(1)	Z	C(2)	N(1)	Y
C(3)	C(1)	Z	C(3)	C(4)	Y
C(4)	C(3)	Z	C(4)	O(4)	Y
H(1)	N(1)	Z	N(1)	C(1)	Y
H(2)	N(1)	Z	N(1)	C(1)	Y
H(3)	N(1)	Z	N(1)	C(1)	Y
H(4)	C(1)	Z	C(1)	C(2)	Y
H(5)	C(3)	Z	C(3)	C(4)	Y
H(6)	C(3)	Z	C(3)	C(4)	Y
H(7)	O(4)	Z	O(4)	C(4)	Y

[a] The AX 1, AX 2 plane is defined by the ATOM 0−ATOM and ATOM 2−ATOM 1 vectors. The third axis is taken perpendicular to this plane, defining a right-handed system.

will be considered. Model **1** corresponds to a "conventional" multipole refinement in which a scale factor, the atomic positions (48), anisotropic (54), and isotropic (7) temperature parameters of the heavy and of the hydrogen atoms, respectively, were refined together with their charge density parameters (216). The pseudoatomic $\rho(\mathbf{r})$ of the NH_3^+ moiety occurred to be over-parametrized by this model, since the refinement did not lead to satisfactory convergence. The ratio of the shifts to the standard uncertainties of the corresponding variables, especially for the valence charges, remained at relatively high values. The distances obtained for the N−H and O−H bonds appeared to be short relative to the values obtained by neutron diffraction.[22]

Table 3. Figures of Merit of Different Refinement Models

	model			
	spherical	m1	m2A	m2B
NREF		7962		
NVAR	89	304	263	284
R(F)	0.0375	0.0287	0.0334	0.0292
$R_w(F)$	0.0410	0.0218	0.0250	0.0223
GOF	4.25	2.29	2.63	2.35

The incorporation of the neutron positional parameters of the hydrogen atoms reduced the number of variables to 303 and led to a stable refinement. However the rigid-bond test[33] indicated that the anisotropic displacement amplitudes (ADP) from the neutron measurement are affected by severe systematic errors. The bond projected components of the mean-square displacement (MSD) tensors for a pair of atoms forming a bond differed by an order of magnitude more than expected from atoms of comparable mass. Thus, instead of making use of the neutron ADPs, the following procedure, referred to as model **2**, has been adopted.

In this refinement the calculated ADPs obtained from ab initio (HF/6-311G**) harmonic force field of the isolated, optimized molecule were used as starting parameters. This requires the transformation of the MSD tensors corresponding to the internal vibrational modes (U_{int}) from the inertial system of the optimized molecule to the crystal system. The transformation was done in two steps. At first the calculated tensors were expressed in local frames used to represent the spherical harmonics (Table 2). These coordinate systems were defined by using the optimized geometrical parameters. In the second step the tensors

(33) Hirshfeld, F. L. *Acta Crystallogr.* **1976**, *A32*, 239.

Table 4. Multipole Populations Based on Model **2B**[a]

	O(1)	O(2)	O(3)	O(4)	N(1)	C(1)	C(2)	C(3)	C(4)
κ	0.979(1)	0.979(1)	0.982(2)	0.996(2)	0.969(3)	1.007(5)	1.008(4)	1.019(5)	0.979(4)
P_v	6.25	6.61	6.22	6.00	5.78	3.79	3.94	3.98	4.23
P_{11}		−0.08	−0.08	−0.04		−0.03			
P_{1-1}				−0.08	−0.04	−0.08	−0.04	−0.04	−0.04
P_{10}	−0.02	0.04	0.05	−0.02	−0.07		−0.02	−0.07	−0.05
P_{20}			−0.04	0.03	−0.08	0.04	−0.02	−0.03	0.09
P_{21}		0.04	0.02	0.04					
P_{2-1}		−0.03	0.05	0.02		0.06	0.04	0.04	0.08
P_{22}	−0.05	−0.05	−0.05	−0.04	0.03	0.05	−0.25	0.04	−0.22
P_{2-2}		−0.02	0.05	0.06	0.05				
P_{30}	−0.02	0.02	0.02		0.21	0.23	0.31	0.21	0.29
P_{31}				0.03		0.06			
P_{3-1}						0.03	0.04		−0.04
P_{32}		−0.03			0.02	0.05	0.24		0.20
P_{3-2}						0.02			
P_{33}	0.05	0.04	0.02	0.08	0.18				
P_{3-3}						−0.21		−0.16	−0.02
P_{40}			−0.03		0.02	0.06		0.03	
P_{41}						0.08			
P_{4-1}	0.04			0.03				−0.04	−0.03
P_{42}	−0.02	−0.02	0.02		−0.02		0.02		
P_{4-2}	0.02		0.02	0.02	−0.03				
P_{43}	−0.02	−0.03	−0.02		−0.07	0.02			
P_{4-3}			−0.04	0.03		0.09	0.04	0.06	−0.03
P_{44}			0.02	0.02		−0.02	−0.04	0.03	0.06
P_{4-4}			−0.02						

	H(1)	H(2)	H(3)	H(4)	H(5)	H(6)	H(7)
κ	1.20	1.20	1.20	1.20	1.20	1.20	1.20
P_v	0.76	0.75	0.60	0.85	0.80	0.80	0.64
P_{10}	0.07	0.01	0.18	0.18	0.09	0.09	0.15
P_{20}							0.25

[a] Only populations for which ($|P_{lm}| > 1\sigma(P_{lm})$) are listed.

were transformed from the local to the crystal system, but here the local frames defined with respect to the experimental molecular configuration were used. This procedure, described in more detail elsewhere,[34] allows one to relate internal ADPs of corresponding atoms of two molecules in slightly different conformations. The calculated MSD tensors at each atomic site, corresponding to the optimized structure, are displayed in Figure 2b in terms of their root-mean-square displacement (RMSD) surfaces defined by $\langle\mu^2\rangle_n^{1/2} = \mathbf{n^T U n}$, where **n** is a unit vector in an arbitrary direction.[35] In Figure 2a the corresponding pattern is seen for the tensors generated for the experimental molecular structure in the way described above. The relative orientations of the surface demonstrates that the transformation of the MSD tensors between the two conformers preserved their local characteristics.

In the first stage of this refinement (**2A**) the shifts in the ADPs were restricted, via rigid-link type constraints,[36] to fulfill the rigid-body motion requirement.[37] This was achieved by invoking $6N-20$ ($N = 16$ is the number of atoms) independent rigid-link constraints, i.e., by keeping the mean-square displacement amplitudes (MSDA) along interatomic links equal for a necessary number of atom pairs (Δ_{ik} MSDA $= 0$). The linearly independent links were derived by means of singular-value decomposition of the matrix of constraints. The procedure, since it corresponds to a fit of the **T**, **L**, and **S** tensors of the rigid-body motion model to the structure factors, gives rise to ADPs for which $U = U_{TLS} + U_{int}$. During this step the C−H, O−H, and N−H distances were kept constant. In the second stage (**2B**) the ADPs of the hydrogen atoms obtained were kept fixed, and the rigid-link conditions were applied only to the C(1)−N(1) bond and to the fragment formed by the C(1), C(2), O(1), O(2) and the C(3), C(4), O(3), O(4) atoms.

The contribution of the internal modes to the ADPs, in terms of U_{eq} ($U_{eq}=1/3(U_{11}+U_{22}+U_{33})$), was found to be in the range of 30−40 and 40−50% for the carbon and oxygens atoms, respectively.

The statistical figures of merit of the different refinements are given in Table 3. The multipole parameters based on model **2B** are listed in Table 4.

Results and Discussion

The inspection of the entries in Table 3 shows that model **1** and **2B** perform almost equally well in fitting the data, although the former one has 20 additional variables. The performance of model **2A** is surprisingly good considering that it has the highest reflections-to-variables ratio.

The differences in the structural data obtained by the different refinements are not significant. Table 5 compares the experimental (model **2B**) and ab initio-optimized geometrical parameters. The carbonyl bond lengths seem to be underestimated by the HF method. Moreover, the theoretical distances of the two C−O bonds in the carboxylate anion deviate from each other to a larger extent than do the corresponding experimental values. This is most likely due to an intramolecular O−H interaction occurring in the optimized structure, where the O(1)···H(1) distance is anomalously short (1.7791 Å) compared to that found in the crystal (2.5712 Å). It is worthwhile mentioning at this point that the optimization at the MP2 level results in the neutral form of the molecule, that is the H(1) atom

(34) Koritsanszky T. *Acta Crystallogr*. in preparation.
(35) Hummel, W.; Hauser, J.; Bürgi, H.-B. *J. Mol. Graphics* **1990**, *8*, 214.
(36) Didisheim, J.-J.; Schwarzenbach D. *Acta Crystallogr*. **1987** A43, 226.
(37) Schomaker, V.; Trueblood, K. N. *Acta Crystallogr*. **1968**, *B24*, 63.

Table 5. Selected Experimental and Optimized Geometrical Parameters

bond distances [Å]	exptl	HF/6-311++G(d,p)
O(1)−C(2)	1.2618(3)	1.2337
O(2)−C(2)	1.2547(3)	1.2055
O(3)−C(4)	1.2261(3)	1.1924
O(4)−C(4)	1.3131(3)	1.3139
N(1)−C(1)	1.4912(3)	1.5032
C(1)−C(2)	1.5366(3)	1.5721
C(1)−C(3)	1.5274(3)	1.5250
C(3)−C(4)	1.5123(3)	1.5068
C(1)−H(4)	1.0602	1.0803
C(3)−H(5)	1.0656	1.0890
C(3)−H(6)	1.0533	1.0803
O(4)−H(7)	1.0336	0.9474
N(1)−H(1)	1.0143	1.0043
N(1)−H(2)	1.0203	1.0295
N(1)−H(3)	1.0131	1.0062
bond angles [deg]	**exptl**	**HF/6-311++G(d,p)**
C(4)−O(4)−H(7)	110.5(1)	109.6
C(1)−N(1)−H(1)	109.9(1)	110.6
C(1)−N(1)−H(2)	111.1(1)	102.0
C(1)−N(1)−H(3)	109.9(1)	113.3
H(1)−N(1)−H(2)	106.8(1)	106.9
H(1)−N(1)−H(3)	108.0(1)	108.3
H(2)−N(1)−H(3)	111.2(1)	115.5
N(1)−C(1)−C(2)	110.2(1)	105.5
N(1)−C(1)−C(3)	111.6(1)	112.1
N(1)−C(1)−H(4)	106.2(1)	108.2
C(2)−C(1)−C(3)	111.8(1)	109.4
C(2)−C(1)−H(4)	108.4(1)	110.8
C(3)−C(1)−H(4)	108.4(1)	110.7
O(1)−C(2)−O(2)	126.0(1)	133.3
O(1)−C(2)−C(1)	116.9(1)	112.4
O(2)−C(2)−C(1)	117.1(1)	114.3
C(1)−C(3)−C(4)	112.3(1)	114.7
C(1)−C(3)−H(5)	110.6(1)	110.5
C(1)−C(3)−H(6)	108.9(1)	107.8
C(4)−C(3)−H(5)	110.1(1)	106.7
C(4)−C(3)−H(6)	109.0(1)	110.4
H(5)−C(3)−H(6)	105.7(1)	106.5
O(3)−C(4)−O(4)	123.8(1)	122.6
O(3)−C(4)−C(3)	122.0(1)	124.2
O(4)−C(4)−C(3)	114.2(1)	113.2
torsional angles [deg]	**exptl**	**HF/6-311++G(d,p)**
N(1)−C(1)−C(2)−O(1)	−6.1(1)	−11.8
N(1)−C(1)−C(2)−O(2)	172.2(1)	170.1
N(1)−C(1)−C(3)−C(4)	−61.5(1)	−57.0
C(3)−C(1)−C(2)−O(1)	118.6(1)	109.0
C(3)−C(1)−C(2)−O(2)	−63.1(1)	−69.1
C(2)−C(1)−C(3)−C(4)	174.6(1)	−173.7
C(1)−C(3)−C(4)−O(3)	2.4(1)	29.8
C(1)−C(3)−C(4)−O(4)	−176.9(1)	−152.4

is transferred to the nearby oxygen leaving a distorted NH_2 moiety. It is also interesting to compare the experimental geometrical parameters of the carboxylate group in L-alanine[8] to those obtained for D,L-aspartic acid. In the former structure the oxygen atom forming the longer bond with the carbon atom is involved in two, whereas the other oxygen, with a shorter C−O bond, only in one intermolecular hydrogen bond. In the crystal structure of aspartic acid the situation is the opposite with a noticeable difference in the strength of the corresponding hydrogen bonds. The oxygen atom (O(1)) of the longer C−O bond is an acceptor in one very strong hydrogen bond characterized by the O(1)···H(7) distance of 1.5222 Å. The C(1)−C(2) distance in the optimized molecule is anomalously long which is most likely due to its extreme polar character suggested by the net atomic charges of −0.04 and 0.2 for the C(1) and C(2) atom, respectively.

The carbon skeleton is shown to be planar in both the experimental and the optimized molecule. The deviation of the calculated molecular conformation from that found in the crystal can be described by rotations of the COO^-, COOH, and the NH_3^+ groups by about 21, 13, and 30° respectively, around the bonds formed with the corresponding carbon atoms. These conformational differences manifest themselves also in the ΔMSDA values shown in Table 6 where the upper (lower) triangular matrix listed here refers to the optimized (experimental) geometry. The matrix appears to be symmetric, especially in the block formed by the C(1) C(2) O(1) O(2), C(3) C(4) O(3) O(4), N(1) H(1) H(2) H(3), and C(3) H(5) H(6) atoms, while the values for some 1−*n* links ($n > 3$) deviate considerably. These findings suggest that the direct applicability of the complete set of rigid-link constraints based on the calculated ADPs and on the experimental conformation is suspect in the present study. Table 7 contains the bond components as well as the Δ MSDAs corresponding to the 1−3 links as obtained in the conventional refinement, by model **1**, and by model **2B**. The values corresponding to the conventional refinement show slight bias, especially for the polar bonds, due to the inadequacy of the spherical-atom model. The Δ MSDAs obtained by the two multipole models are in good agreement; only small deviations can be found for some 1−3 links. Based on these numbers it can be concluded that the relevance of refinement **2B** lies mainly in the possibility of assigning physically meaningful ADPs to the hydrogen atoms.

The topological analysis of the theoretical densities was performed with the program PROAIM,[38] while the experimental $\rho(\boldsymbol{r})$ was analyzed with the property program XDPROP of the system XD.[29] In both cases the Laplacians were evaluated; all bond CPs, all bonded valence shell charge concentrations (VSCC, the (3,+3) CPs of $\nabla^2\rho(\boldsymbol{r})$), and all but one expected nonbonded VSCCs were located.

Figure 3 compares the negative Laplacian functions, in the plane of the COO^- and COOH groups, calculated from the wave function at HF/6-311++(3df,3pd) level and from the static $\rho(\boldsymbol{r})$ based on model **2B**. The topological equivalence of the functions obtained by the two methods is evident in both the bonding and nonbonding areas. In the bonds the charge concentrations form continuous regions between the atoms which is a characteristic feature of covalent interaction. A quantitative comparison of the results can be given in terms of bond topological properties. In Table 8 the $\rho(\boldsymbol{r}_b)$ and $\nabla^2\rho(\boldsymbol{r}_b)$ values, the bond ellipticities, and the differences (l_b-r) between the bond path length l_b and the geometrical bond lengths r are listed. The trend in the theoretical values clearly shows the effect of high angular momentum basis functions, i.e., the more extended the basis is the more charge concentration is found in the bond. The differences in the strengths of the covalent bonds revealed in the $\rho(\boldsymbol{r}_b)$ values appear to have chemical relevance. The carboxyl carbonyl bond (C(4)−O(3)) possesses higher bond order than those in the carboxylate group (C(2)−O(1) and C(2)−O(2)) and the $\rho(\boldsymbol{r})$ in these bonds is higher than in the C−OH single bond (C(4)−O(4)). For the bonds formed by the non-hydrogen atoms model **1** and **2B** give significantly the same (within their standard uncertainties) topological parameters. This is not true for the O−H and C−H bonds which is due to the different treatment of the hydrogen atoms in the two refinements. The theoretical bond parameters, referred to in the following discussion, correspond to the calculations at the HF/6-311++(3df,3pd) level. For the polar bonds (C−O and C−N) the

(38) Cheeseman, J.; Keith, T. A.; Bader, R. F. W. AIMPAC program package. McMaster University: Hamilton, Ontario, 1992.

Table 6. Difference Mean-Square Displacement Amplitude Matrix for Internal Motions [10^4 Å^2][a]

	O1	O2	O3	O4	N1	C1	C2	C3	C4	H1	H2	H3	H4	H5	H6	H7
O1		0	10	−1	0	−1	1	−2	−4	212	225	115	95	121	123	61
O2	0		0	−10	4	−2	0	−13	−15	202	173	73	104	153	120	34
O3	12	5		1	−3	−14	−12	−2	1	61	307	321	118	104	84	124
O4	−5	−9	1		13	−1	−4	−4	0	57	238	328	132	107	110	38
N1	8	5	2	12		−1	−5	−3	−15	53	42	41	82	149	62	83
C1	−1	−2	−14	2	−2		1	1	−1	85	82	78	47	88	88	69
C2	2	1	−12	−4	−7	1		0	−2	204	177	78	95	134	128	56
C3	−6	−8	−1	−4	−4	−3	1		−2	78	139	175	85	48	47	51
C4	−5	−15	1	0	−18	−2	−2	−2		57	255	314	136	93	89	75
H1	284	180	156	86	52	74	198	54	97		30	−19	−10	27	−14	35
H2	315	181	219	275	43	87	199	155	253	20		−16	3	65	−68	−169
H3	47	70	132	255	39	82	59	193	231	−25	−16		−19	−44	−80	−235
H4	88	114	124	136	86	50	94	87	139	4	11	−32		0	32	−46
H5	116	154	94	110	155	86	136	49	92	95	19	−103	−2		−8	−50
H6	124	113	93	107	60	86	128	46	91	13	−63	−108	32	−7		−67
H7	53	47	121	38	81	67	56	50	71	−19	−204	−101	−50	−62	−58	

[a] Upper (lower) triangular matrix refers to the optimized (experimental) geometry.

Table 7. Δ MSDAs for Selected Bonds and 1−3 Links

	model		
bonds	m1	m2B	spherical
C(2)−O(1)[a]	0	2	4
C(2)−O(2)[a]	−1	1	6
C(4)−O(3)[a]	2	1	6
C(4)−O(4)[a]	1	0	5
C(1)−C(2)[a]	0	1	0
C(1)−C(3)	0	−1	−2
C(3)−C(4)[a]	−2	−2	0
C(1)−N(1)[a]	1	−2	2
	model		
1−3 links	m1	m2B	spherical
O(1)−O(2)[b]	0	0	−1
O(1)−C(1)[b]	0	−1	2
O(2)−C(1)[b]	−3	−2	−4
O(3)−O(4)[b]	−1	1	−2
O(3)−C(3)[b]	0	−1	−1
O(4)−C(3)[b]	1	−4	1
C(2)−C(3)	2	0	1
C(2)−N(1)	−6	−7	0
C(1)−C(4)	1	1	0
C(3)−N(1)	2	1	4

[a] Constrained in model 2B. [b] Constrained in model 2B.

experiment gives somewhat higher $\rho(\boldsymbol{r}_b)$ and considerably higher $-\nabla^2\rho(\boldsymbol{r}_b)$ than the theory, whereas for the C−C bonds the opposite trend is seen. In Table 8 the locations of the bond CPs are also given in terms of their distances d from the first atom defining the bond. The experimental minima of $\rho(\boldsymbol{r})$ are found to be closer to the more electronegative atom than are the theoretical ones. As illustrated in Figure 4 for the C(4)−O(3) bond, the locations of the bond CP of the multipole $\rho(\boldsymbol{r})$ is close to the bonded VSCC, i.e., to the point where $-\nabla^2\rho(\boldsymbol{r})$ exhibits a local maximum. Here a relatively small change in the position of the CP is accompanied by a significant change in $-\nabla^2\rho(\boldsymbol{r})$. For the most extended calculation (HF/6-311++G-(3df,3dp)) the bond properties were evaluated also at the experimental location of the bond CPs, and thus the values obtained can directly be compared to those derived from the multipole model density. In this case the experimental and theoretical values of the Laplacian are in fair agreement. All of these findings are in good accord with those discussed earlier in the study on L-alanine.[8] The fact that the location of the bond CP correlates with the polar character of the bond has been realized and used as a measure of the bond-polarity.[39]

Table 8. Topological Parameters of Bonds Formed by Non-Hydrogen Atoms[a]

bond	ρ	$\nabla^2\rho$	ϵ	d	$(l_b - r)$	method
O(1)−C(2)	2.55	−8.9	0.03	0.842		HF/6-311++G(d,p)
	2.61	−17.6	0.08	0.839		(2d,2p)
	2.65	−16.9	0.08	0.841	0.000 18	(3df,3pd)
	2.67	−30.1	0.11	0.801		(3df,3pd)
	2.71	−37.6	0.22	0.800	0.001 2	model 2B
O(2)−C(2)	2.60	−9.7	0.05	0.836		(d,p)
	2.67	−18.4	0.10	0.832		(2d,2p)
	2.70	−17.6	0.10	0.835	0.000 23	(3df,3pd)
	2.76	−33.5	0.13	0.764		(3df,3pd)
	2.87	−36.1	0.29	0.763	0.0023	model 2B
O(3)−C(4)	2.74	−4.6	0.04	0.818		(d,p)
	2.82	−13.6	0.10	0.815		(2d,2p)
	2.86	−13.4	0.09	0.818	0.000 16	(3df,3pd)
	2.88	−29.0	0.12	0.784		(3df,3pd)
	2.96	−42.2	0.21	0.784	0.00 19	model 2B
O(4)−C(4)	2.17	−2.6	0.12	0.888		(d,p)
	2.24	−11.1	0.05	0.885		(2d,2p)
	2.26	−10.6	0.05	0.887	0.000 66	(3df,3pd)
	2.34	−27.8	0.06	0.803		(3df,3pd)
	2.41	−29.7	0.06	0.803	0.000 91	model 2B
N(1)−C(1)	1.54	−3.4	0.11	1.019		(d,p)
	1.57	−10.7	0.08	1.002		(2d,2p)
	1.58	−8.1	0.08	1.012	0.000 14	(3df,3pd)
	1.65	−14.8	0.01	0.868		(3df,3pd)
	1.69	−12.9	0.09	0.868	0.01 38	model 2B
C(1)−C(2)	1.76	−18.3	0.06	0.840		(d,p)
	1.74	−16.6	0.07	0.818		(2d,2p)
	1.78	−18.9	0.08	0.829	0.000 71	(3df,3pd)
	1.79	−18.2	0.10	0.766		(3df,3pd)
	1.69	−12.9	0.25	0.766	0.01 14	model 2B
C(1)−C(3)	1.73	−16.7	0.03	0.778		(d,p)
	1.71	−15.2	0.04	0.774		(2d,2p)
	1.75	−17.1	0.03	0.775	0.0 01	(3df,3pd)
	1.74	−16.9	0.02	0.784		(3df,3pd)
	1.61	−12.1	0.04	0.784	0.00 36	model 2B
C(3)−C(4)	1.81	−19.1	0.09	0.677		(d,p)
	1.80	−17.7	0.08	0.695		(2d,2p)
	1.84	−19.6	0.09	0.682	0.000 27	(3df,3pd)
	1.84	−19.2	0.08	0.723		(3df,3pd)
	1.70	−12.2	0.03	0.723	0.00 17	model 2B

[a] ρ and $\nabla^2\rho$ denote the electron density and Laplacian at the bond CP, ϵ is the bond ellipticity, d is the distance from the first atom defining the bond to the bond CP, and $l_b - r$ is the difference between the bond path length and geometrical bond distance. The fourth entry for each bond refers to values at the experimental location of the bond CP. Units are in e and Å.

The theoretical and experimental topological indices associated with the π and bent character of the bonds show considerable discrepancies. The bond ellipticity (ϵ) for carbonyl

(39) Cremer, D.; Kraka, E. *Croat. Chem. Acta* **1984**, *57*, 1259.

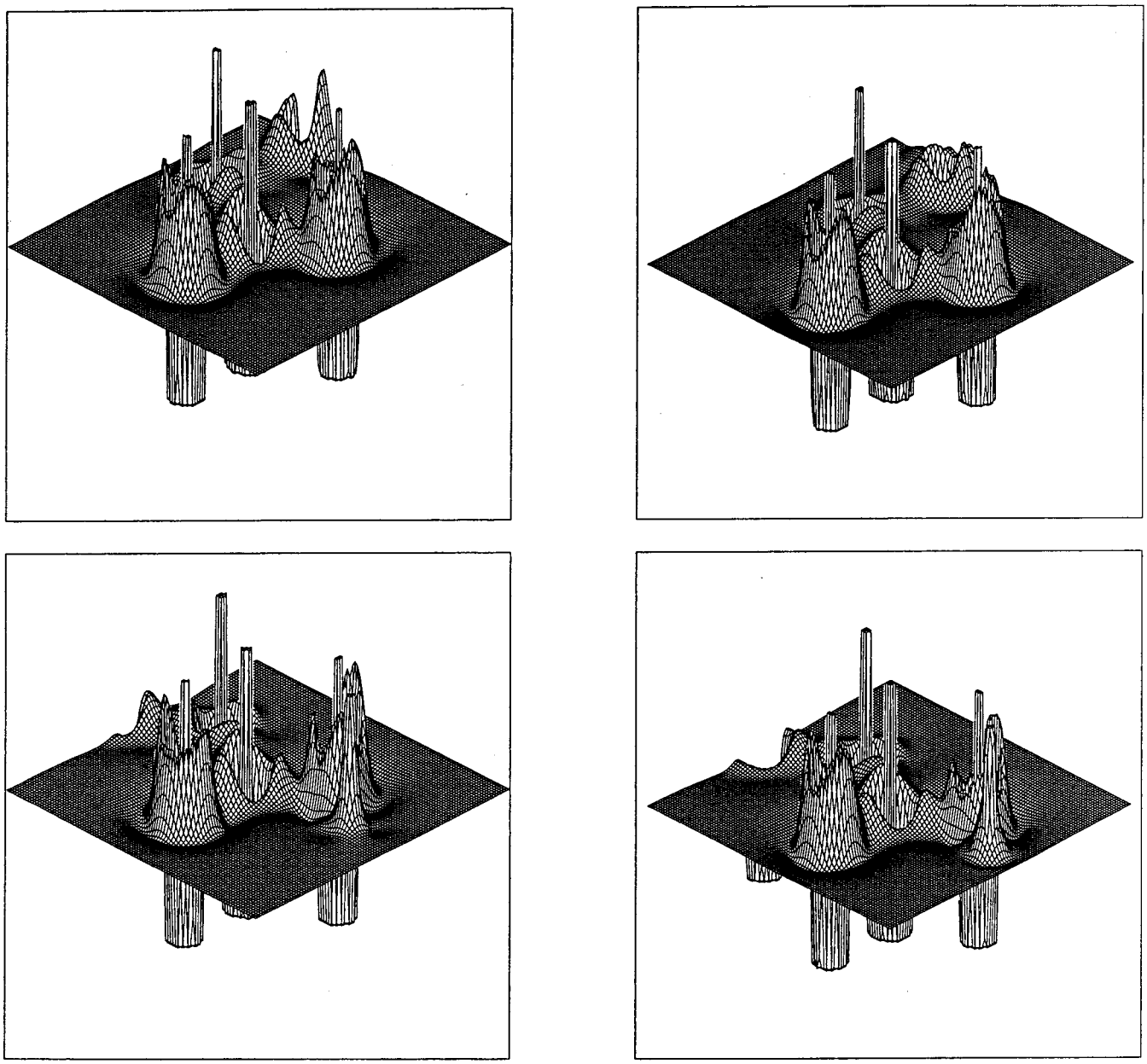

Figure 3. Relief maps of the negative Laplacian functions in the plane of the COO^- (top) and COOH group (bottom) obtained from experiment (based on model 2B, left) and from the wave function (right).

bonds has been found also in the range of 0.2−0.3 in several experimental studies[8,9,12,13] (for the C═C bond in ethylene ϵ = 0.41 at MP2/6-31+G** level). The extent of conjugation of the carbonyl bonds into the adjacent C(1)−C(2) bond is also in line with previous experimental results. Although, these values describe the expected π character of these bonds reasonably well, they are typically 3 to 4 times larger than those found theoretically. The l_b-r quantities are at least an order of magnitude larger for the experimental than for the theoretical density. This discrepancy suggests that the displacements of experimental bond CPs relative to their theoretical location occur not only along the interatomic vectors but also in other directions.

Table 9 compares experimental $\rho(\mathbf{r}_b)$ and $\nabla^2\rho(\mathbf{r}_b)$ values for selected polar bonds, obtained for L-alanine[8] (23K), methylammonium hydrogen succinate[9] (110 K), potassium hydrogen(+)-tartrate[12] (15 K) and (2*S*)-3-(3′,4′-dihydroxyphenyl)alanine (L-dopa),[13] with our results for D,L-aspartic acid. The overall agreement is satisfactory, especially if we consider all chemical and structural differences between these molecular systems which are expected to affect the local density distribution of the bonds selected. If the correlation between the bond distances and the corresponding $\rho(\mathbf{r}_b)$ values is taken into account the bond densities agree within their estimated uncertainities. Even for the Laplacian a fair quantitative agreement is found and only a few outliers can be detected.

The geometrical and topological parameters of the O···H−X (X = O, N, C) hydrogen bonds are listed in Table 10. The oxygen atoms O(1) and O(4) are acceptors in one, O(2) and O(3) in two hydrogen bridges. O(3) and O(4) are also bonded to C−H donors with O···H distances shorter than the sum of the van der Waals radii (2.6 Å). Characteristic of closed shell interactions are the low density and the positive Laplacian at the CP which are reproduced by the experimental values in Table 10. The stronger the bond the higher the density located between the O and H atoms. It is important to note that (3,−1) CPs could be located also in O···H−C contacts. For the strong (weak) hydrogen bonds the interaction path length is

Table 9. Experimental Bond Distances (R) and Bond-Topological Parameters of Selected Polar Bonds[a]

compound	T [K]	C···O R	C···O ρ	C···O $\nabla^2\rho$	C=O R	C=O ρ	C=O $\nabla^2\rho$	C−OH R	C−OH ρ	C−OH $\nabla^2\rho$	C−N R	C−N ρ	C−N $\nabla^2\rho$
aspartic acid	20	1.2618	2.87	−36.1	1.2261	2.96	−42.2	1.3131	2.41	−29.7	1.4912	1.69	−12.9
		1.2547	2.71	−37.6									
alanine[8]	23	1.267	2.86	−29.6							1.488	1.70	−11.1
		1.248	3.02	−39.0									
hydrogen tartrate[12]	15	1.2720	2.65	−39.5	1.2196	2.89	−32.3	1.3178	2.28	−28.9			
		1.2492	2.74	−34.8									
methylammonium hydrogen succinate[9]	110	1.286	2.52	−29.7							1.480	1.63	−12.1
		1.245	2.86	−35.4									
(2*S*)-3-(3′,4′-dihydroxyphenyl)alanine (L-dopa)[13]	173	1.260	2.84	−38.8							1.495	1.62	−8.4
		1.258	2.70	−32.6									

[a] Units are e and Å.

Table 10. Experimental Geometrical and Bond-Topological Parameters for Hydrogen Bonds[a]

A···H−D	symm. op./transl.	R(A···D)	R(A···H)	α (A···H−D)	ρ	$\nabla^2\rho$	R(A−CP)	R(CP-bond)
O(1)···H(7)−O(4)	1/2+x, 1/2−y, 1/2+z 0 0 0	2.5556(3)	1.5222(2)	178.6(1)	0.50(1)	1.1(2)	1.050	0.014
O(2)···H(1)−N(1)	x, −y, 1/2+z 0 1 0	2.8197(3)	1.8075(2)	175.5(1)	0.25(1)	3.6(2)	1.153	0.012
O(2)···H(2)−N(1)	1/2−x, 1/2+y, 1/2−z 1 0 1	2.8629(3)	1.8480(2)	172.7(1)	0.26(1)	3.2(2)	1.159	0.012
O(3)···H(3)−N(1)	−x, y, 1/2−z 1 0 0	2.8904(3)	1.9794(2)	148.3(1)	0.10(1)	2.2(2)	1.276	0.219
O(3)···H(4)−C(1)	−x, −y, −z 1 1 1	3.3368(3)	2.5033(2)	134.9(1)	0.04(1)	0.8(2)	1.489	0.213
O(4)···H(6)−C(3)	−x, y, 1/2−z 1 0 1	3.3111(3)	2.5621(2)	127.6(1)	0.04(1)	0.7(2)	1.469	0.141

[a] Units are e, Å, and deg. R(A···H) and R(A−CP) are the distances of the acceptor atoms from the hydrogen atom and from the CP of the A···H interaction, respectively. R(CP-bond) denotes the distance of the CP from the A···H intermolecular vector. α(A···H−D) is the angle formed by the acceptor, hydrogen, and donor atoms.

Table 11. Nonbonded Valence Shell Charge Concentrations of Oxygen Atoms[a]

atom	r		$\nabla^2\rho$		R		C−O−CP		CP_1−O−CP_2	
O(1)	6.53	5.79	−134.4	−122.7	0.340	0.347	104.8	108.1		
	5.75	5.72	−110.7	−116.3	0.348	0.348	107.4	116.2	147.25	119.7
O(2)	6.72	6.29	−140.9	−136.3	0.358	0.343	103.9	121.9		
	5.74	6.10	−114.0	−123.1	0.347	0.346	109.5	114.3	144.8	112.1
O(3)	6.22	6.01	−123.2	−121.1	0.345	0.342	110.9	107.6		
	6.35	6.27	−127.0	−146.9	0.344	0.352	107.9	143.4	141.2	109.1
O(4)	7.20	6.48	−146.6	−143.5	0.335	0.339	106.8	122.0		

[a] In each column the left (right) entries are theoretical (experimental) values. Units are e, Å, and deg. R is the radial distance of the (3,+3) CP of the Laplacian from the oxygen atom, C−O−CP is the angle formed by the C−O bond and the O−CP vector, CP_1 −O−CP_2 is the angle formed by the CP_1−O and O−CP_2 vector.

slightly (considerably) longer than the geometrical length of the interaction line connecting the donor with the acceptor. Table 11 compares the theoretical and experimental nonbonded VSCCs in terms of the $\rho(\boldsymbol{r})$ and $\nabla^2\rho(\boldsymbol{r})$ values at the (3,+3) CPs of the Laplacian. Curiously, the numerical procedure applied was unable to locate the second nonbonded VSCC for the oxygen atom of the hydroxyl group (O(4)). The geometrical arrangements of the lone-pairs at each oxygen atom are also given by the O−CP distances, the C−O−CP, and the CP_1−O−CP_2 angles. Both $\rho(\boldsymbol{r})$ and $\nabla^2\rho(\boldsymbol{r})$ values obtained by the two methods agree within 10%. It is to note that for O(1) which is the acceptor in the strongest hydrogen bridge the experimental Laplacian at the (3,+3) CP increases from −116.3 to −98.0 e/Å^5 if the corresponding symmetry generated molecule (1/2+x, 1/2−y, 1/2+z) is included in the calculation. This effect for the other oxygen atoms involved in weaker hydrogen bonds or short contacts turns out to be negligible.

The dipole and quadrupole moments of the molecule extracted from the crystal field (Table 12) seem to display the effect of intermolecular interactions. The experimental dipole moments obtained by a measurement in the solution[40] and by the diffraction method agree very well, whereas the theoretical values referring to an isolated molecule are smaller by about 2 Debye which is a typical deviation found in several studies.[41] The polarization of the molecular electron density in the crystal,

Table 12

a. Dipole Moments[a]

method	dipole moment
multipole model **2B**	13.4(8)
solution measurement[39]	13.1
HF/6-311++G(d,p)	11.60
HF/6-311++G(2d,2p)	11.40
HF/6-311++G(3df,3pd)	11.33

b. Quadrupole Moments[b]

	HF/6-311++G(3df,3pd)	model **2B**
xy	−41.47	−49.46
xz	−121.53	−127.14
yz	−43.31	−45.17
(xx−yy)/2	−64.53	−61.27
3zz-rr	−116.89	−97.65

[a] Unit in D. [b] Unit in DÅ.

(40) Khanarian G.; Moore W. J. *Aust. J. Chem.* **1980**, *33*, 1727.
(41) Spackman, M. A. *Chem. Rev.* **1992**, *92*, 1769.

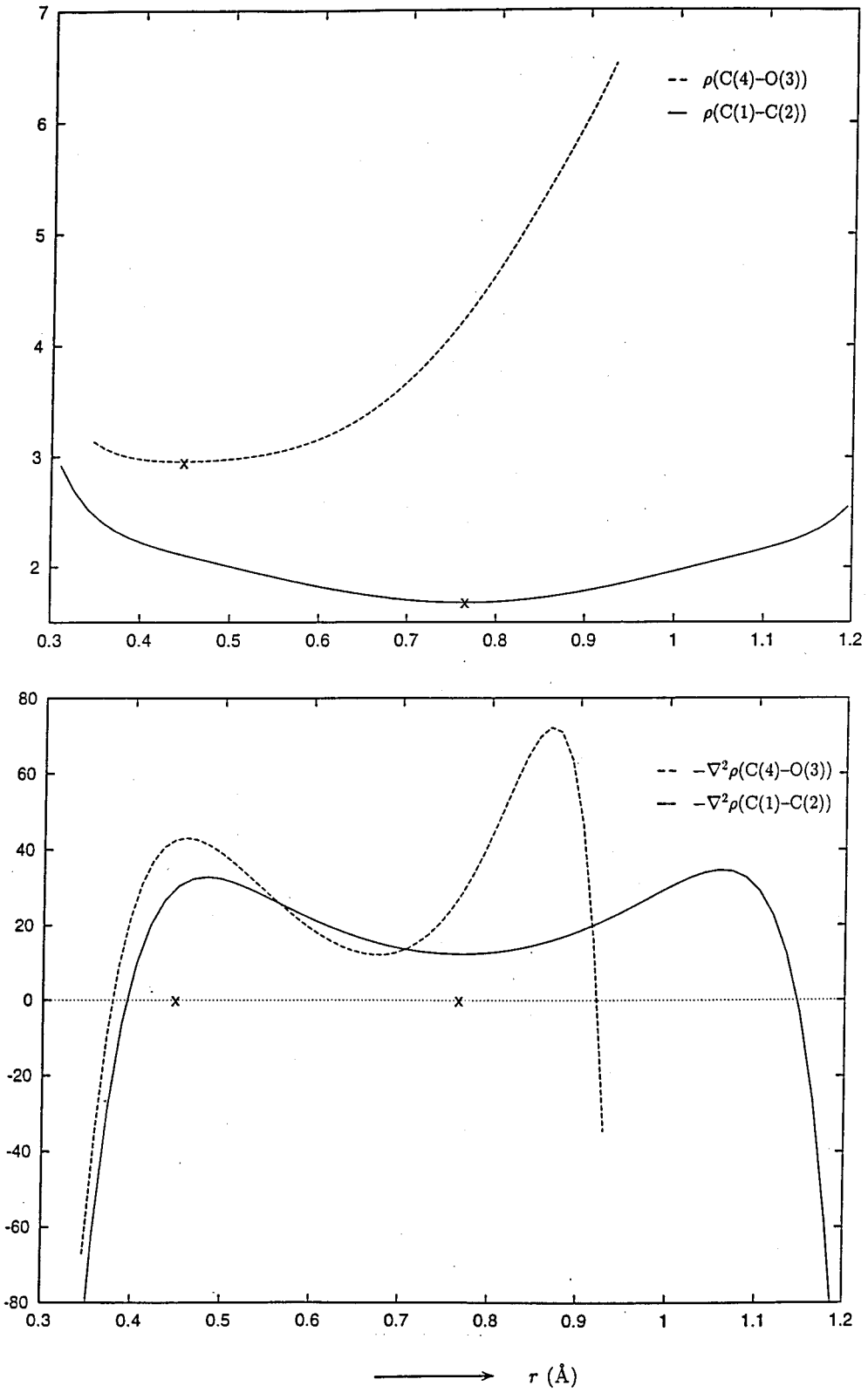

Figure 4. Distribution of the experimental $\rho(r)$ and $-\nabla^2\rho(r)$ along the bond paths of the C(4)−O(3) and C(1)−C(2) bonds. Crosses mark the locations of the critical points.

suggested by the enhanced dipole moment, seems to be accompanied by its slight contraction due to hydrogen bonding, as seen in the second moments listed in Table 12.

The EP was calculated from model **2B** using the method of Su and Coppens[42] which permits the correct evaluation of this function at any position. The experimental equipotential map seen in Figure 5a is based on the monomolecular density, i.e., it corresponds to the molecule isolated from the crystal structure, and it is to be compared with the map calculated from the wave function (Figure 5b). The dominating feature of these maps is the continuous electronegative region around the carboxylate group. Here, similarly to the situation found for L-alanine,[8] the experimental EP is more diffuse than that derived at the HF

(42) Su, Z. W.; Coppens, P. *Acta Crystallogr.* **1992**, *A48*, 188.

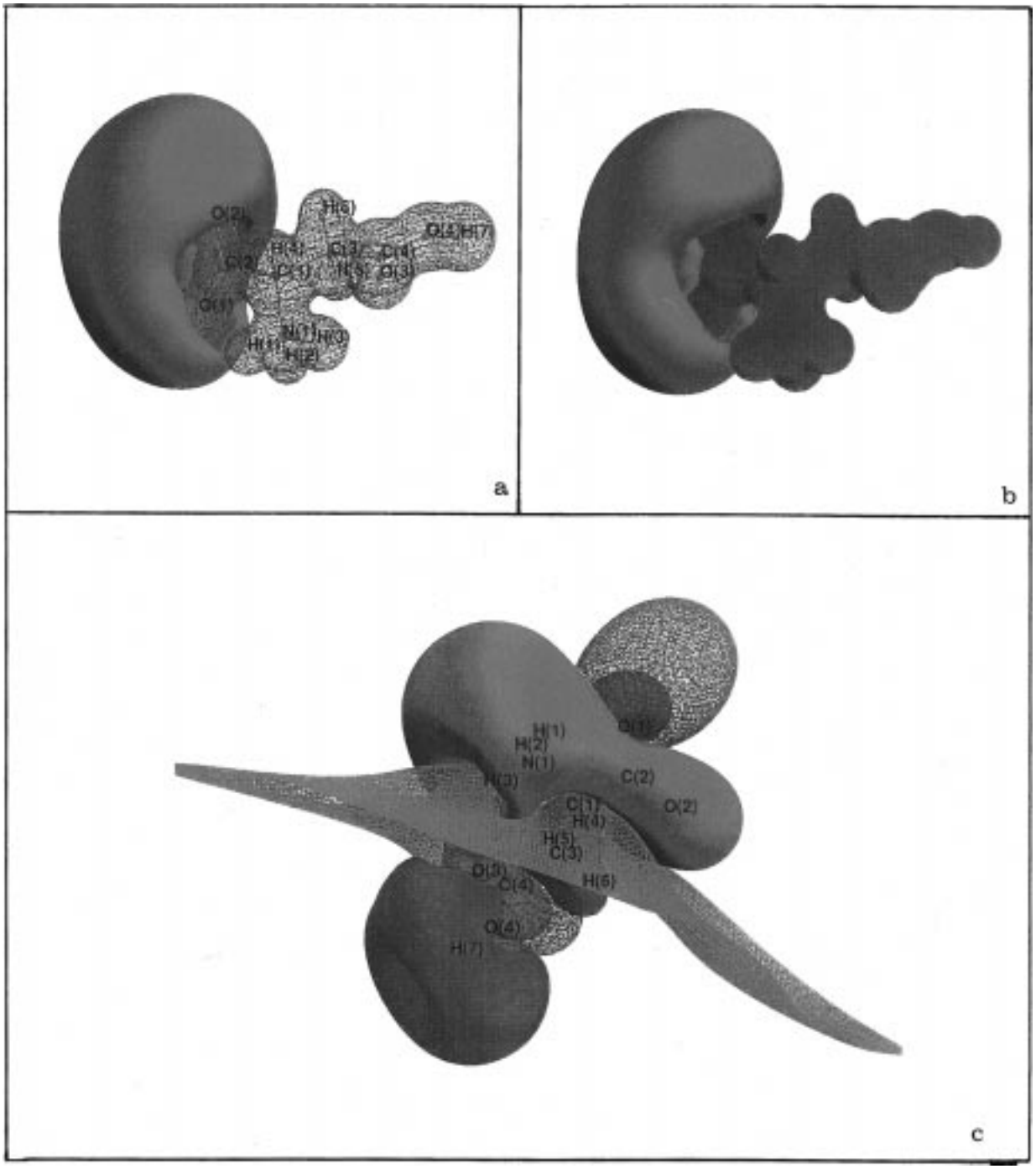

Figure 5. 3D graphical representation of the electrostatic potential calculated from the experimental monomolecular density (a) and wave function (b). Difference between the experimental and theoretical EPs (c). The following equipotential surfaces are displayed: (a,b) red −0.1 *e*/Å, blue 0.5 *e*/Å. (c) red −0.05 *e*/Å, blue 0.05 *e*/Å, green: zero surface.

level of theory. More details are seen in Figure 5c where the difference between the experimental and theoretical functions is displayed in terms of equipotential surfaces. There are two distinct zero potential surfaces. One of them encloses the atom O(1) with a positive residual potential. The other one separates the negative region, formed by the O(2), C(2), C(4), N(1), H(1), and H(2) atoms, from the positive region of the rest of the molecule. The red surface of −0.05 *e*/Å represents that region in space where the experimental EP is less positive or more negative than the theoretical one. The former situation applies to the NH_3 group, while the ones to the C(2)═O(2) carbonyl group. The blue surface of 0.05 *e*/Å corresponds to a positive residual EP and encloses that region of space where the experimental EP is more positive or less negative than the theoretical one. If we assume that the theoretical EP describes the free molecule correctly and that the corresponding experimental function is an unbiased estimate of the EP of a molecule "removed" from the crystal, then the residual EP shown in Figure 5c represents the genuine polarization caused by the crystal field.

Conclusion

From the analysis of the charge distribution and related electronic properties of aspartic acid, derived from high resolution X-ray diffraction data and from the wave function at the HF level, the following points emerge.

As reported earlier in several studies of the same type, the theoretical $\rho(\boldsymbol{r})$ of the isolated molecule is topologically

equivalent to that extracted from the crystal through modeling the diffraction pattern. This means that the number and types of CPs of $\rho(\boldsymbol{r})$ found for the energy-optimized stationary system at the experimental nuclear arrangement are the same as obtained for the molecule being in thermal equilibrium in the crystalline state. Even the Laplacian functions derived by the two methods exhibit qualitatively equivalent features of atomic interaction in the bonded as well as in the nonbonded regions of the valence shell.

A quantitative comparison of the theoretical and experimental density, as discussed earlier,[8] is subject to many conditions. The locations of the minima of $\rho(\boldsymbol{r})$ along the bond paths can differ markedly for the two densities, especially in polar bonds. Since $\rho(\boldsymbol{r})$ usually posesses a flat minimum between atoms sharing the electrons, $\rho(\boldsymbol{r}_b)$, an important indicator of the strength of the interaction, is quite insensitive to the location of the minimum. That is why the $\rho(\boldsymbol{r}_b)$ parameters are usually in good accord (within the estimated experimental error) with the theoretical values and seem to be obtained "reliably" from diffraction experiments. This can also be true for the Laplacian for a bond formed by equivalent atoms in which case $-\nabla^2\rho(\boldsymbol{r})$ exhibits a plateau between the two bonded VSCCs. For a polar bond the CP can be close to the location of one of the maxima of the Laplacian where the positive curvature changes rapidly. In the pseudoatom model applied, the spherical atomic valence densities are the main contribution to the total $\rho(\boldsymbol{r})$ of light atoms and thus the valence charges are expected to be the dominating parameters in determining the location of the bond CPs. The application of a statistical analysis[43] to the multipole refinement shows that, although the number of reflections affecting the estimates of the static density parameters are the highest for the monopoles, this set of datapoints have almost equal influence on all of them. In other words, the "charge sensitive" reflections have weak selectivity and contribute almost equally to the estimates of individual monopoles. As a consequence, the main components of the eigenvectors corresponding to the smallest eigenvalues of the conditioned[44] LSQ matrix are the shifts of the atomic valence charges, indicating that only certain linear combinations of the monopoles are obtainable and their individual values are less significant. Based on this mathematical analysis, it is usually not possible to reveal the physical meaning of the parameter independencies involved but constraints suggested by simple arguments are expected to increase the condition number of the LSQ matrix and thus to support a chemically relevant solution. In aspartic acid one can, for example, assign +1 and −1 electron net charges to the NH_3^+ and COO^- groups, respectively, and keep them fixed during the refinement. In addition, the COOH and CH_2 groups can be kept neutral. These restrictions led to a model density which reproduced the topology of the polar bonds better than that given by model **2B**. The C(4)−O(3) bond, for example, becomes even more polarized (0.34 electron is transferred from the carbon to the oxygen atom) due to the group charge constraints. As a result, $\nabla^2\rho(\boldsymbol{r})$ increases from −42.2 to −32.0 *e*/Å.[5] Such applications are to be explored in more detail which is certainly out of scope of this paper.

Another model inadequacy of similar nature is connected to the problem of thermal deconvolution. The analysis of the experimental $\rho(\boldsymbol{r})$ of potassium hydrogen(+)-tartrate[12] gave relatively high charge concentrations in the C−O and O−H bonds, and the Laplacian at the CPs of these bonds became even more negative when more high-order data were included in the refinement. This tendency was accompanied by a considerable bias in the ADPs which did not satisfy the rigid bond condition. If a bond was forced to satisfy this criterion the bond curvature of $\rho(\boldsymbol{r})$ showed less sensitivity to the refinement conditions. The incorporation of information on the internal vibrational motion into the refinement by means of a set of properly chosen rigid-link constraints is not a straightforward procedure, but it turns out to be important. In the case of aspartic acid the parameter estimates given by the unconstrained refinement seemed to be less biased than those found for the hydrogen(+)-tartrate ion, and no direct correlation between the treatment of the ADPs and the location of the bond CPs could be shown. Nevertheless, the treatment of the hydrogen atoms at the level of the anisotropic thermal motion model is likely to be essential in deriving "reasonable" atomic monopoles. This is because the charge transfer in organic molecules occurs basically at the expense of charge of the hydrogen atoms.

All of these remarks could let us draw a somewhat compromising conclusion that the theory and experiment can or even have to lead to considerably different CP locations in polar bonds, that is, to different results for Bader's partitioning. The fact that theoretical and experimental densities, because of their different nature, are indeed not comparable, has been stressed by several authors.[45,8] The extent to which fine details in the gradient field of $\rho(\boldsymbol{r})$ affect integrated atomic properties should certainly be the subject of further studies. To explore the reliability of the experimental method, in terms of the topology of the $\rho(\boldsymbol{r})$ obtained, seems to remain of great importance. The concordance between these parameters obtained for the C═O bonds in different molecules, from different quality and resolution X-ray data, treated and interpreted in certainly different ways, is rather promising and seems to carry valuable chemical information.

Despite the differences in the local topological features of the densities compared, their integrated electronic properties, such as the first and second moments, were found to be in excellent agreement.

The analysis of the nonbonded interactions in terms of the topology of the experimental $\rho(\boldsymbol{r})$ delivered chemically significant results, and the effect of the crystal field on the Laplacian was also detectable. These findings certainly verify the importance of experimental charge density determinations. In the course of our ongoing studies on amino acids, aiming at systematic analysis of their electron density in the crystalline state, we expect to be able to draw more general conclusions than those presented here.

Acknowledgment. This work was funded by the Bundesminister für Bildung, Wissenschaft, Forschung und Technologie (BMBF), Bonn, Germany (Grant no. 05 647KEA1) and by the Fonds der Chemischen Industrie, Frankfurt, Germany.

Supporting Information Available: Tables of crystal data and structure refinement, atomic coordinates, bond lengths and angles, anisotropic displacement parameters, and hydrogen coordinates and isotropic displacement parameters and structure of aspartic acid (6 pages). See any current masthead page for ordering and Web access instructions.

JA972620E

(43) Prince, E.; Nicholson, W. L. In Structure and Statistics in Crystallography; Wilson, A. J. C., Ed.; Adenine Press: New York, 1985; p 183.

(44) Prince, E.; Boggs, P. T. International Tables for X-ray Crystallography; Kluwer Academic Publishers: 1992; Vol. C., p 594.

(45) Stewart, R. F. In The Application of Charge Density Research to Chemistry and Drug Design, NATO-ASI Series B; Jeffrey, G. A., Piniella, J. F., Eds.; Plenum Press: New York, 1991; Vol. 250, p 63.

(46) Keller, E. SCHAKAL88. User manual. University of Freiburg: Germany, 1988.